Direct Power Control of a Doubly Fed Induction Generator with a Fixed Switching Frequency

Won-Sang Kim, Sung-Tak Jou, Kyo-Beum Lee
School of Electrical and Computer Engineering
Ajou University, Suwon, Korea
kyl@ajou.ac.kr

Steve Watkins
Fleadh Electronics Ltd

***Abstract* — This paper presents the implementation of a direct active and reactive power control of a doubly fed induction generator (DFIG) applied to a wind generation system as an alternative to the classical field oriented control (FOC). The FOC is known to have complex control structure, which consists of current controller, power controller and frame transformations, and also depend highly on parameter variation such as rotor and stator resistances and inductances. The proposed direct power control (DPC) method produces a fast and robust power response without calling for complex structure and algorithms. However, it has high power ripple during steady state. In this paper, active and reactive power controllers and space-vector modulation (SVM) are combined to replace the hysteresis controllers used in the original DPC drive, resulting in the fixed switching frequency of power converter. The simulation results with FOC and DPC for a 3kW DFIG are given and discussed and experimental results for the same machine are shown to illustrate the feasibility of the proposed control strategy.**

Keywords-direct power control, doubly fed induction generator, field oriented control, frame transformation, parameter variation, space-vector modulation, hysteresis controllers, fixed swithing frequency

I. INTRODUCTION

The concept of a doubly fed induction generator applied to a wind generation system is an interesting option with a significant market potential. This system allows variable speed operation over a large, but restricted range. The most important merits of variable speed wind turbines compared to conventional fixed speed wind turbines are increased energy capture, improved power quality and reduced mechanical stress on the wind turbine [1].

A DFIG consists of a wound rotor induction generator (WRIG) with the stator windings directly connected to a three-phase power grid and with the rotor windings mounted to a bidirectional back-to-back IGBT frequency converter. A schematic diagram of variable speed wind turbine system with a DFIG is shown in Fig. 1.

The power converter consists of the rotor-side converter and the grid-side converter, in which the rotor-side converter controls the active and reactive power and the grid-side converter controls the DC-link voltage and ensures a converter operation at unity power factor [2]. Control of a DFIG is traditionally achieved through the control of the components of the voltage vector in a field-oriented control (FOC), which is achieved by a rotor current controller [3-6]. One main draw back of this system is that its performance depends greatly on accurate machine parameters such as stator, rotor resistances, and inductances.

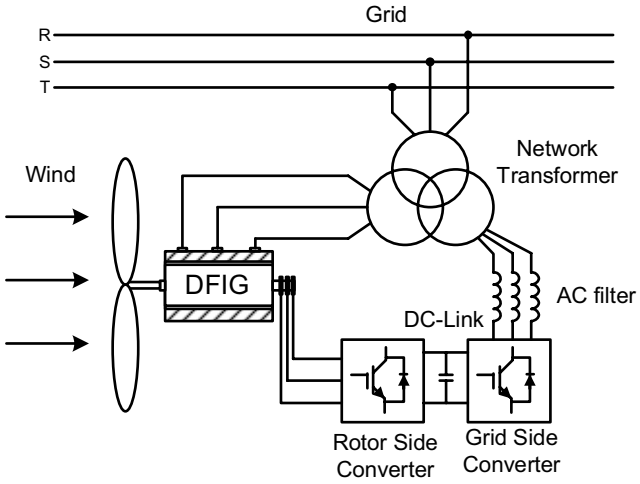

Fig. 1. Schematic diagram of variable speed wind turbine system with a DFIG.

Thus, performance degrades when actual machine parameters depart from values used in the control system. Direct power control (DPC) abandons the rotor current control philosophy, characteristic of FOC and achieves bang-bang active and reactive power control by modulating the rotor voltage in accordance with the active and reactive power errors. DPC is characterized by fast dynamic response, simple structure and robust response against parameter variations. It does not employ a rotor current controller and SVM [7], [8]. One drawback with the basic DPC is that it displays large current, active and reactive power ripple, resulting in vibration and acoustic noise. Another drawback for DPC is converter switching frequency variation that significantly complicates power circuit design. In order to obtain a smooth operation and fixed switching frequency, direct power control is

978-1-4244-2279-1/08/$25.00 © 2008 IEEE

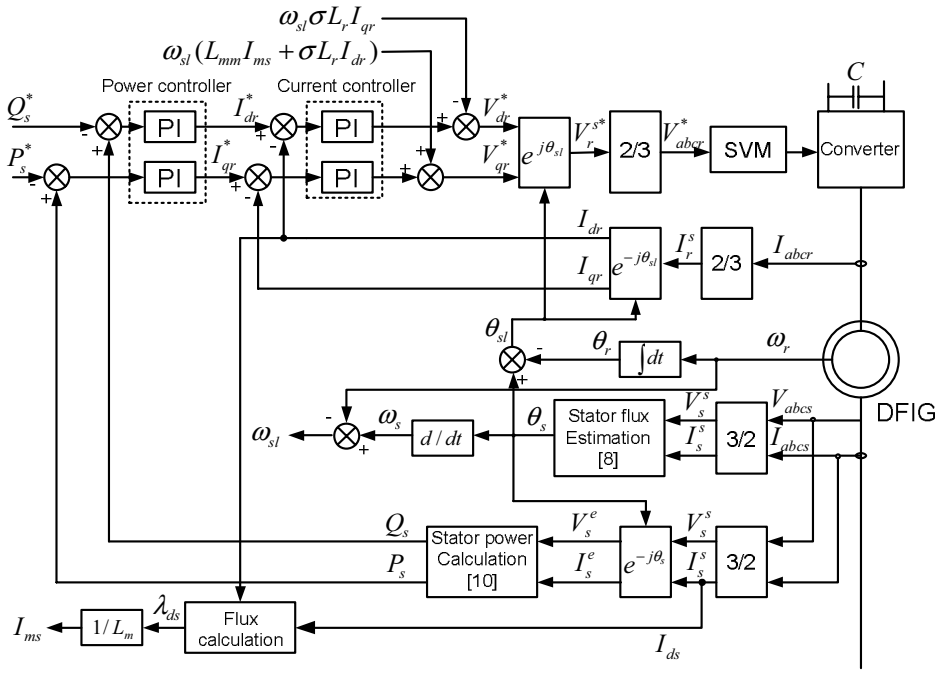

Fig. 3. Field oriented control (FOC) structure for the rotor side converter of a DFIG.

combined with a SVM strategy based on the principles of the DPC method.

This paper presents a new direct active and reactive power control based on SVM for a DFIG-based wind turbine system. The control strategy directly calculates reference rotor control voltage with each switching period, using the estimated stator flux, the calculated active and reactive powers and their errors. Simulation results for a 3 kW are shown to demonstrate and experimental results for a 3 kW are shown to demonstrate the performance of the proposed control strategy.

II. FOC REVIEW

A. Modeling of the DFIG

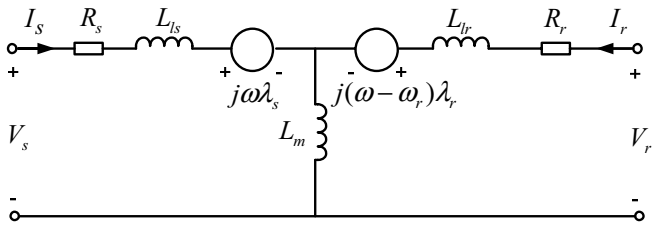

Fig. 2. An equivalent circuit in the arbitrary reference frame.

The DFIG is a wound rotor induction generator, in which the rotor circuit is connected to the grid through two back-to-back converters with a common DC link capacitor bank. The ability to subtract and supply power from the rotor makes it possible to operate the DFIG at sub-synchronous or super-synchronous speed while keeping a constant voltage and frequency on the stator [9].

The d-q model in the arbitrary reference frame is expressed as follows.

$$V_s = R_s I_s + \frac{d\lambda_s}{dt} + j\omega\lambda_s \tag{1}$$

$$V_r = R_r I_r + \frac{d\lambda_r}{dt} + j(\omega-\omega_r)\lambda_r \tag{2}$$

$$\lambda_s = \lambda_{ds} + j\lambda_{qs}, \quad \lambda_r = \lambda_{dr} + j\lambda_{qr}$$
$$\lambda_{ds} = L_s I_{ds} + L_m I_{dr}, \quad \lambda_{qs} = L_s I_{qs} + L_m I_{qr} \tag{3}$$
$$\lambda_{dr} = L_r I_{dr} + L_m I_{ds}, \quad \lambda_{qr} = L_r I_{qr} + L_m I_{qs}$$

where I_{ds}, I_{qs}, I_{dr}, I_{qr} and λ_{ds}, λ_{qs}, λ_{dr}, λ_{qr} are the currents and the fluxes of the stator and rotor in d- and q-axes, R_s and R_r are the resistances of the stator and rotor windings, ω_r is the rotor speed.

An equivalent circuit is set up by means of the voltage and flux equations of the arbitrary reference frame, as shown in Fig. 2.

B. FOC for the DFIG

The rotor-side converter is controlled in a synchronously rotating dq-axis frame, with the d-axis oriented along the stator flux vector position. In this way, a decoupled control between the stator active and reactive powers is obtained. The influence of the stator resistance can be neglected and stator flux can be constant as the stator is connected to the grid. For such a reference frame selection, the DFIG model can be derived as

$$V_{ds}=0,\ \ V_{qs}=\omega_s\lambda_{ds} \tag{4}$$

$$V_{dr}=(R_r+R_s\frac{L_m^2}{L_s^2})I_{dr}+\sigma L_r\frac{dI_{dr}}{dt}-\omega_{sl}\sigma L_r I_{qr}$$

$$V_{qr}=(R_r+R_s\frac{L_m^2}{L_s^2})I_{qr}+\sigma L_r\frac{dI_{qr}}{dt}+\omega_{sl}(L_{mm}I_{ms}+\sigma L_r I_{dr}) \tag{5}$$

$$\lambda_{ds}=L_mI_{ms}=L_sI_{ds}+L_mI_{dr},\ \ \lambda_{qs}=L_sI_{qs}+L_mI_{qr}=0 \tag{6}$$

$$\lambda_{dr}=\frac{L_m^2}{L_s}I_{ms}+\sigma L_rI_{dr},\ \ \lambda_{qr}=\sigma L_rI_{qr} \tag{7}$$

where $\sigma=1-L_m^2/L_sL_r$, $L_{mm}=L_m^2/L_s$, $\omega_{sl}=\omega_s-\omega_r$ is the slip frequency, ω_s is the electrical angular velocity of the stator, I_{ms} is the magnetizing current of the generator.

The DFIG stator active and reactive powers may be computed as follows.

$$P_s=\frac{3}{2}(V_{ds}I_{ds}+V_{qs}I_{qs})=-\frac{3}{2}\frac{L_m}{L_s}V_{qs}I_{qr}$$
$$Q_s=\frac{3}{2}(V_{qs}I_{ds}-V_{ds}I_{qs})=-\frac{3}{2}V_{qs}(\frac{V_{qs}}{\omega_sL_s}-\frac{L_m}{L_s}I_{dr}). \tag{8}$$

Due to constant stator voltage, the stator active and reactive powers are controlled via I_{qr} and I_{dr} respectively. In the DFIG voltage equation (5), the rotor currents I_{qr} and I_{dr} can be controlled using V_{qr} and V_{dr} respectively. The control scheme consists of inner current controller and outer power controller. Fig. 3 shows the FOC scheme for the rotor-side converter of a DFIG.

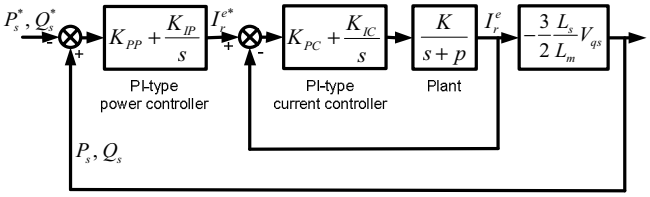

Fig. 4. Overall control system for the FOC.

The pole-placement method is utilized to design PI-controllers in current control loops and power control loops [11]. Consequently, the resulting overall control system implemented on the DFIG corresponds to the block diagram sketched in Fig. 4. It is seen from the control system that all the plants for the current control loop are stable with only one single dominant nonzero pole. In this condition, a straightforward approach for designing a PI-controller is to place the zero of the PI-controller to approximately cancel the dominant pole of the plant, resulting in the closed-loop transfer function of the overall control system.

$$\frac{P_s}{P_s^*}=\frac{Q_s}{Q_s^*}$$
$$\approx\frac{\frac{3}{2}\frac{L_s}{L_m}V_{qs}K_{PP}K_{PC}K(s+\frac{K_{IP}}{K_{PP}})}{s^2+(K_{PC}K+\frac{3}{2}\frac{L_s}{L_m}V_{qs}K_{PP}K_{PC}K)s+\frac{3}{2}\frac{L_s}{L_m}V_{qs}K_{IP}K_{PC}K}. \tag{9}$$

As can be seen from (9), the variation of machine parameters, especially mutual inductance, has impact on the power dynamics.

III. Proposed DPC strategy for the DFIG

In the proposed control strategy, the d-axis of the synchronous frame is fixed to the stator flux, as shown in Fig. 5. Since the stator is directly connected to the grid, and the influence of the stator resistance can be neglected, the stator flux can be considered constant.

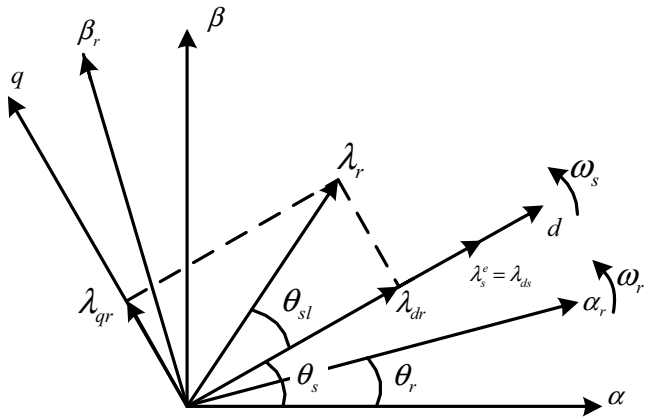

Fig. 5. Stator and rotor flux vectors in the synchronous d-q frame.

From (1), for a synchronous frame ($\omega_e=\omega_s$ - the stator flux speed, $\lambda_s^e=\lambda_{ds}$), the stator voltage vector is given as

$$V_s^e=V_{qs}=\omega_s\lambda_{ds}. \tag{10}$$

Based on (3), the stator current is given by

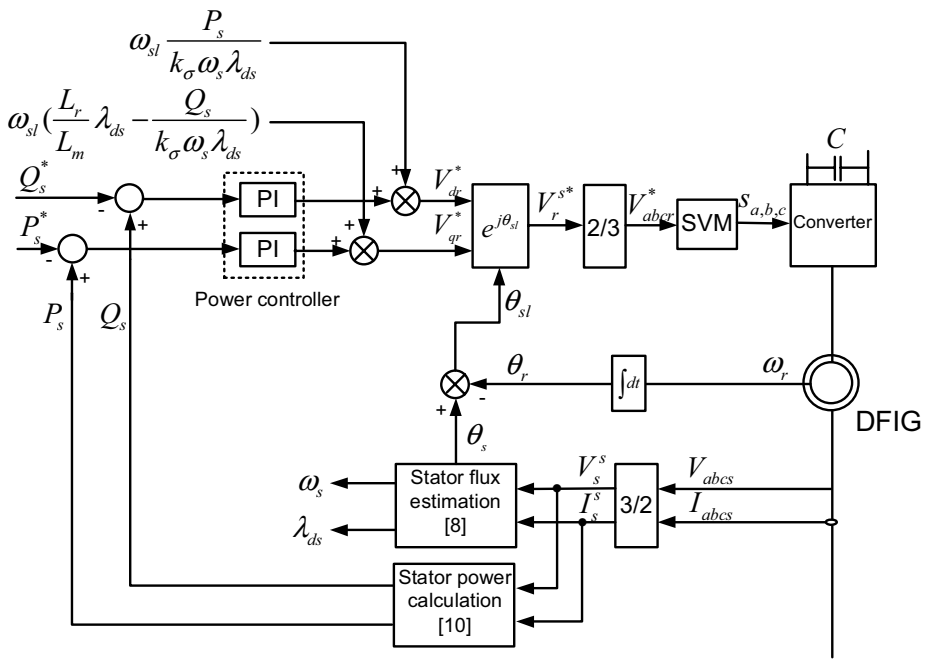

Fig. 6. Schematic diagram of the proposed DPC for a DFIG system.

$$I_s^e = \frac{L_r\lambda_s^e - L_m\lambda_r^e}{L_sL_r - L_m} = \frac{\lambda_s^e}{\sigma L_s} - \frac{L_m\lambda_r^e}{\sigma L_sL_r}. \tag{11}$$

Using (8) and (11), the stator active and reactive power inputs from the network can be calculated as

$$\begin{aligned} P_s &= -k_\sigma\omega_s\lambda_{ds}\lambda_{qr} \\ Q_s &= k_\sigma\omega_s\lambda_{ds}(\frac{L_r}{L_m}\lambda_{ds} - \lambda_{dr}) \end{aligned} \tag{12}$$

where $k_\sigma = 1.5L_m/(\sigma L_sL_r)$.

Since the stator flux remains constant, according to (12), the active and reactive power changes over a constant period of T_s are given by

$$\begin{aligned} \Delta P_s &= -k_\sigma\omega_s\lambda_{ds}\Delta\lambda_{qr} \\ \Delta Q_s &= -k_\sigma\omega_s\lambda_{ds}\Delta\lambda_{dr}. \end{aligned} \tag{13}$$

As shown in Fig. 5, in the synchronous d-q reference frame, the rotor voltage is given by

$$V_r^e = R_rI_r^e + \frac{d\lambda_r^e}{dt} + j\omega_{sl}\lambda_r^e. \tag{14}$$

Combining (12), (13) and (14) and neglecting the rotor resistance, the rotor voltage required to eliminate the power errors in the d-q reference frame is calculated as

$$\begin{aligned} V_{dr} &= (K_{PQ} + K_{IQ}/s)(Q_s - Q_s^*) + \omega_{sl}\frac{P_s}{k_\sigma\omega_s\lambda_{ds}} \\ V_{qr} &= (K_{PP} + K_{IP}/s)(P_s - P_s^*) + \omega_{sl}(\frac{L_r}{L_m}\lambda_{ds} - \frac{Q_s}{k_\sigma\omega_s\lambda_{ds}}). \end{aligned} \tag{15}$$

The first terms on the right-hand side reduce power errors while the second terms compensate for the rotor slip that causes the different rotating speeds of the stator and rotor fluxes. As can be seen, calculations require only simple multiplications and no complicated mathematics.

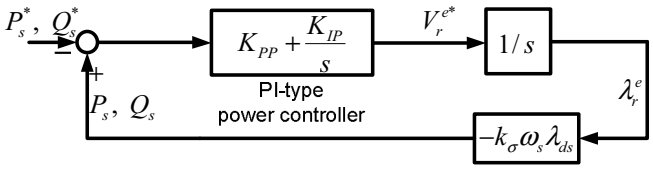

Fig. 7. Overall control system for the DPC.

The schematic diagram of the proposed DPC for a DFIG system is shown in Fig. 6. The controller contains two PI controllers, -one for active power and one for reactive power-, and a SVM unit. The stator active and reactive powers can be calculated directly. The stator flux is estimated using the

measured stator voltages and currents in the stationary reference. Considering (12), (14) and (15), block diagram displays the dynamics existing between P_s and V_{qr}^*, on the one hand, Q_s and V_{dr}^*, on the other hand. The overall control structure of a DPC is essentially constituted by one power controller. Fig. 7 evidences that both dynamics turn out to be exactly the same. Furthermore, this stator flux may be regarded as a constant disturbance, whose effect on Q_s may be easily removed just by closing the reactive power control-loop via a compensator including an integral action.

It is fundamental to note that the error signals feeding the PI controller are computed by subtracting the set-point of the variable to be controlled - Q_s^* or P_s^* - from its actual value - Q_s or P_s, respectively. This is due to the fact that and are strictly negative. As a result, both Q_s and P_s closed-loop dynamics can be represented by the unique second-order transfer function given next.

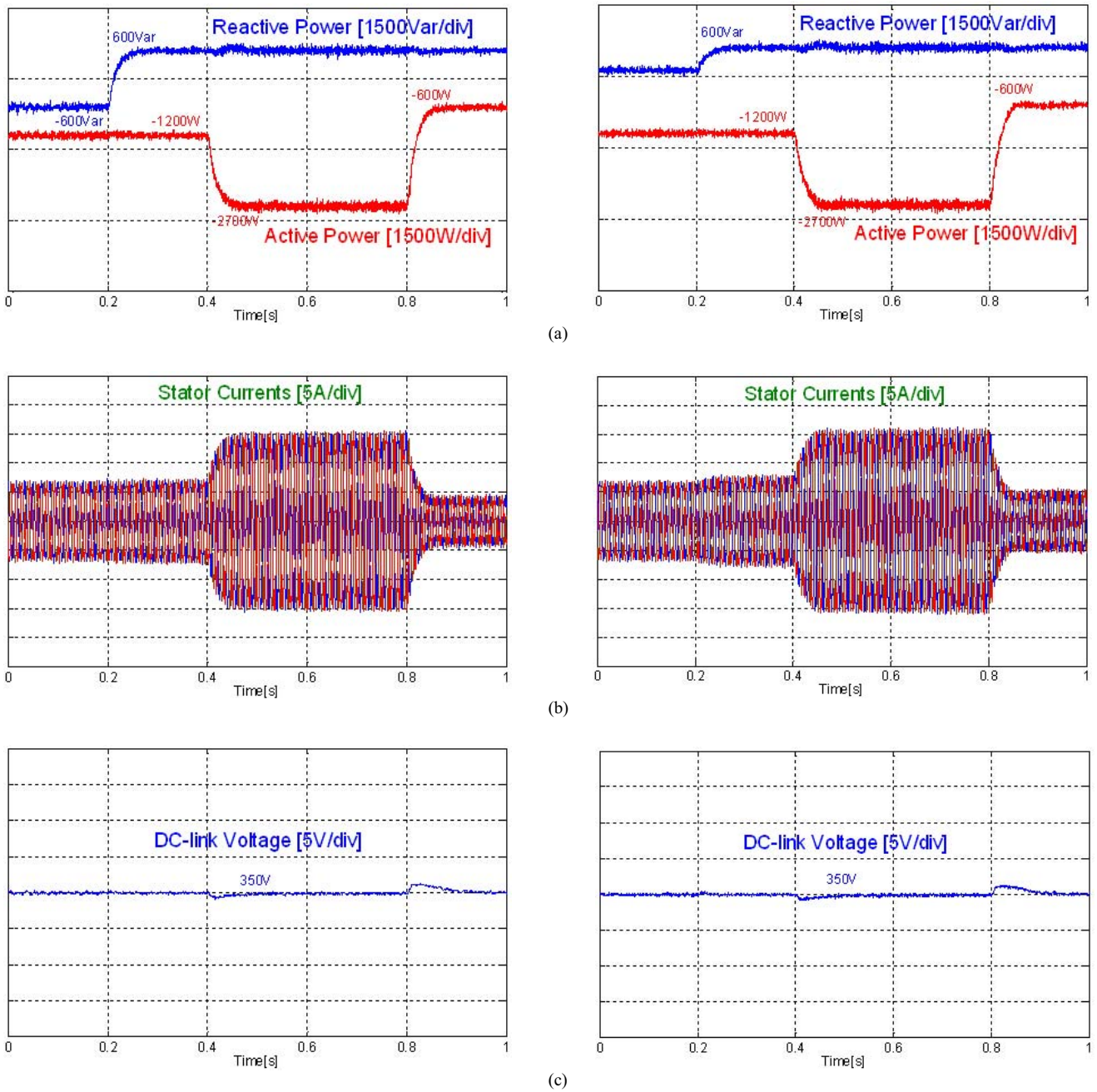

(A) With nominal L_m (B) With 0.5 L_m

Fig. 8. Simulation results of power step responses (a), stator currents (b) and DC-link voltage (c) in the FOC drive.

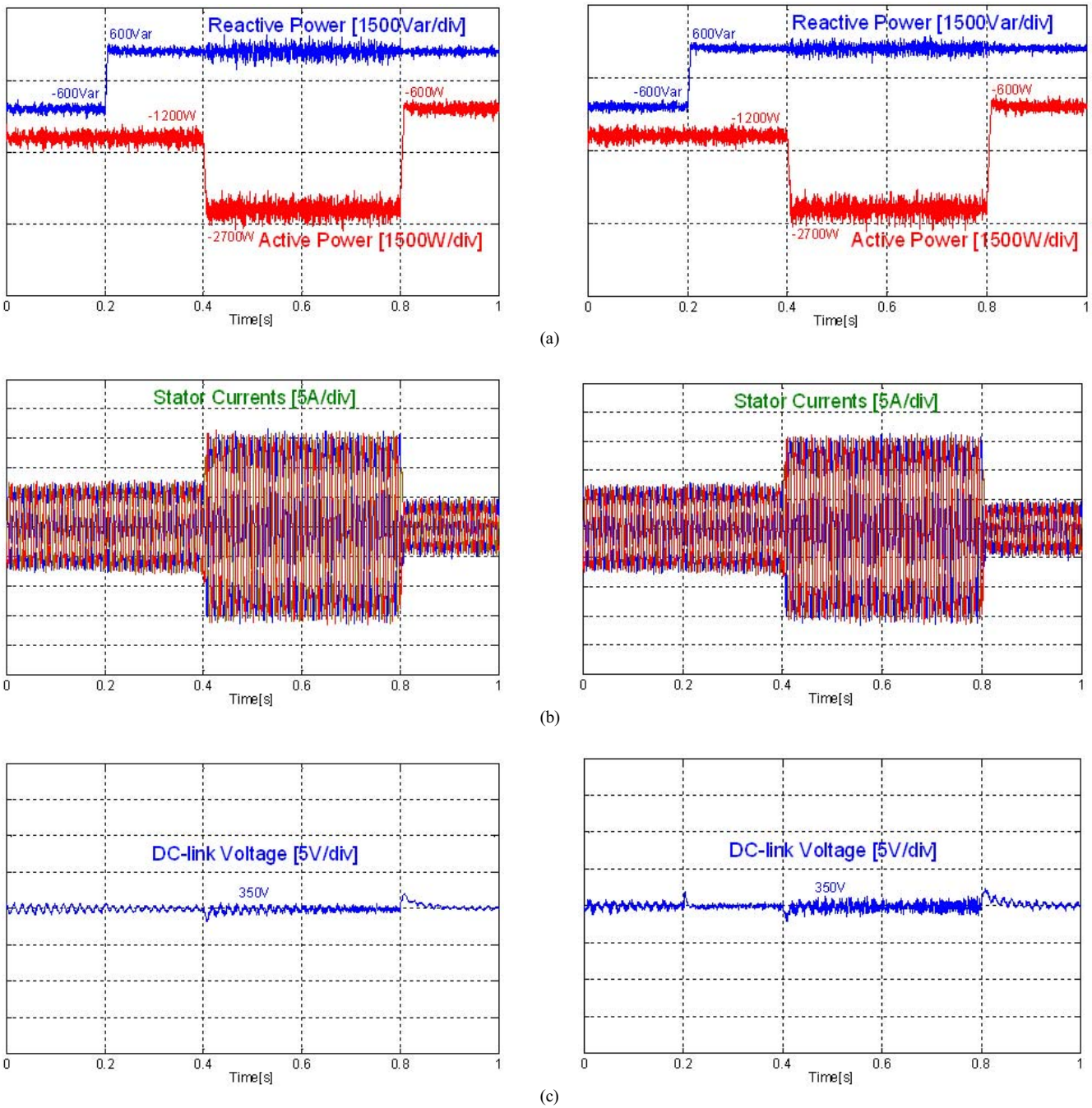

(a)

(b)

(c)

(A) With nominal L_m (B) With 0.5 L_m

Fig. 9. Simulation results of power step responses (a), stator currents (b) and DC-link voltage (c) in the DPC drive.

$$\frac{P_s}{P_s^*} = \frac{Q_s}{Q_s^*} \approx \frac{K_{PP} k_\sigma \omega_s \lambda_{ds} (s + \frac{K_{IP}}{K_{PP}})}{s^2 + K_{PP} k_\sigma \omega_s \lambda_{ds} s + K_{IP} k_\sigma \omega_s \lambda_{ds}} \tag{16}$$

From the transfer function (16), dynamics can be mainly influenced by the constant k_σ that are determined by the stator and rotor leakage and mutual inductance. Substituting stator and rotor inductances (3), the parameter k_σ is rewritten as follow.

$$k_\sigma = \frac{3}{2} \frac{L_m}{L_s L_r - L_m^2} \approx \frac{3}{2} \frac{1}{L_{ls} + L_{sr}} \tag{17}$$

Since the leakage path is mainly air, the variation of machine parameter has little impact on the power dynamics.

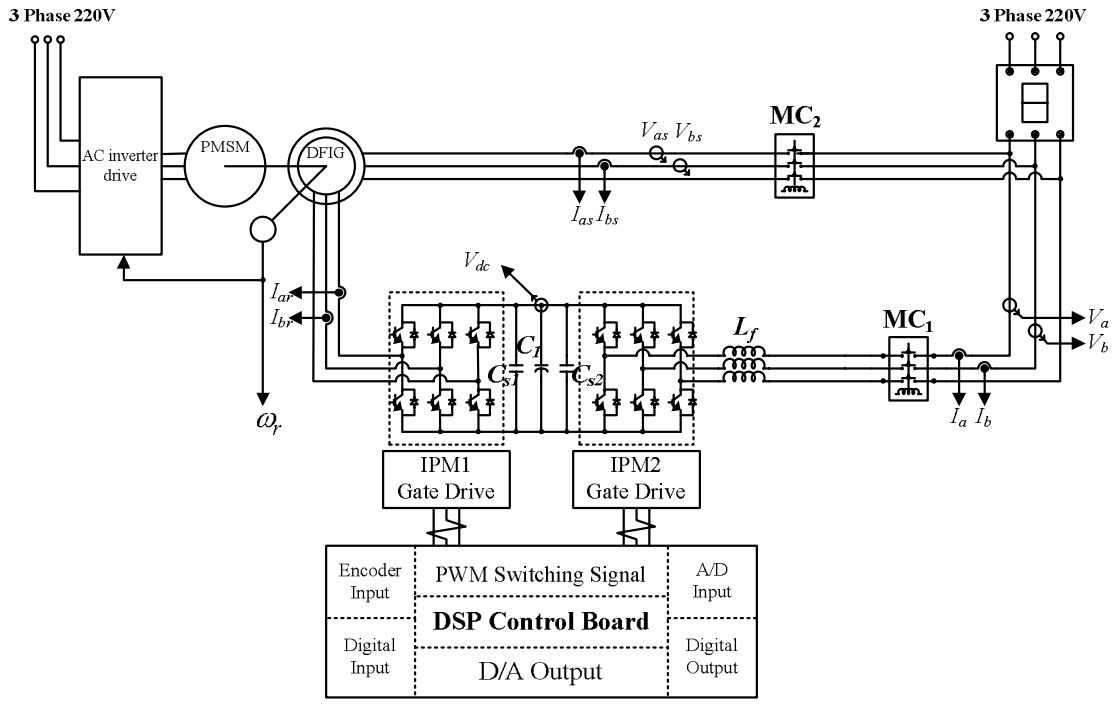

(a) Schematic diagram of the experimental setup.

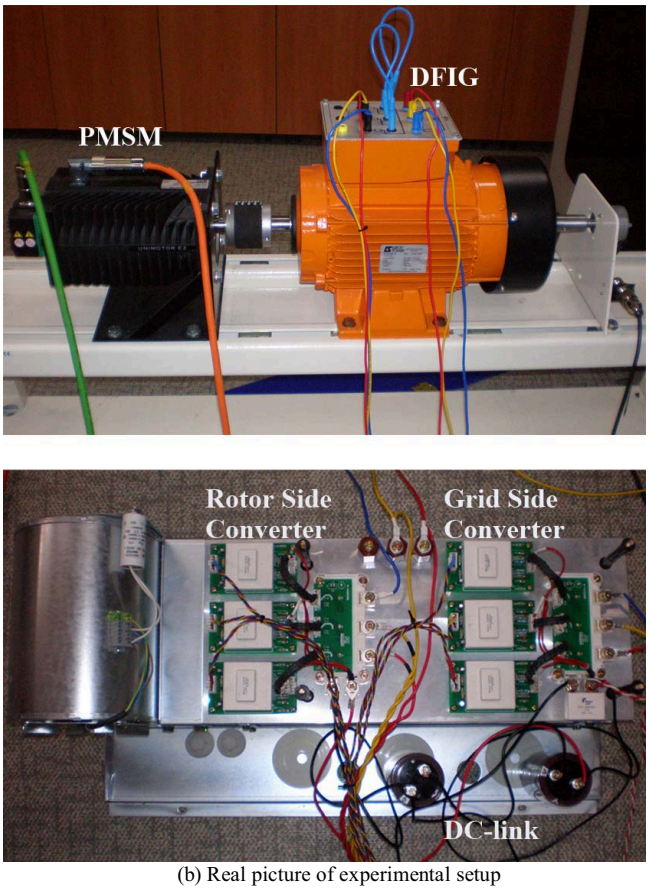

(b) Real picture of experimental setup

Fig. 10. Experimental setup of the DPC system.

IV. Simulation Results

Simulation of the proposed control strategy for a DFIG-based generation system is performed to show that the DPC drive is able to operate with fast dynamic response and robustness of reactive and active power control in comparison with the conventional FOC drive. The DPC and FOC strategies are simulated for a 3kW, 220V, 14.7A, 60Hz four-pole machine and the parameters $R_s = 0.667\Omega$, $R_r = 0.625\Omega$, $L_s = 67.3mH$, $L_r = 67.3mH$ and $L_m = 63.7mH$.

Fig. 8 and 9 show power responses of the FOC drive and the DPC drive when the active and reactive powers are step changed from -600Var to 600Var at 0.2s and from -1200W to -2700W at 0.4s, respectively ("-" refers generating active power and absorbing reactive power). An improve operation in terms of fast dynamic response can be noticed with DPC.

The FOC drive is sensitive to changes in the mutual inductance as shown in Fig. 8(A) and (B). In Fig. 8(B), the reactive power deviates from the control when the reference power -600Var is applied and the overshoot of both the stator currents and the active power occurs under transient conditions. However, Fig. 9(A) and (B) show the robustness of the DPC drive when the mutual inductance has L_m and $0.5L_m$ respectively. It does not depend on the mutual inductance variation and has a robust characteristic against parameter variation.

V. Experimental Results

The experimental setup of the DPC system is shown in Fig. 10. The rated values and parameters of a DFIG are same as the simulation. The generator is driven by 4.96kW, 220V, 3000rpm PMSM fed by an AC inverter. The power electronic stages consist of two back-to-back converters using intelligent power modules (IPM). The rotor-side voltage source PWM converter is inserted in the rotor winding and the grid-side voltage source PWM converter is connected to the stator winding via an AC filter.

The converters are 3kW rated IGBT bridges with a 2400μF DC-link capacitor, whose sampling time is 200μs and switching frequency is 5kHz. The digital controller is based on a digital signal processor (TMS320VC33 DSP) and a 12-bit analog-to-digital (A/D) converter providing fast processing for floating-point calculations. Hall sensors are employed in the current measurement, and the reference voltages are synthesized from the regulated DC-link voltage and SVM signals of the converters. Sampling time during the experiment is 100μs and the rotor side converter switching time is 200μs. Deadtime compensation is also included.

During the experiment, two processes are carried out before the stator winding is connected to the grid via a magnetic contactor (MC). Firstly, at lower rotor speeds, the power generation from DFIG is not enough to supply to the grid. The magnetic contactor is activated when the rotor speed reaches a set rotor speed. Secondly, the stator winding is connected to the grid when the stator voltage, frequency and phase are aligned to the grid. Fig. 11 shows that the stator winding is connected to the grid within 0.24 s. The DPC controller gains used are as follows:

$$K_{PQ} = 0.5,\ K_{IQ} = 500,\ K_{PP} = 0.5,\ K_{IP} = 500;$$

To verify the proposed control strategy, the experimental investigation is focused on the active and reactive power response and the stator current ripple. The active and reactive power references are step changed from -3kW to -2.2kW at 0.5 s and from -0.2kVar to 0.9kVar at 0.7 s, respectively. It is noted that there is no overshoot during transient operation and the steady-state error is maintained constant. The effectiveness of the proposed DPC strategy is confirmed in Fig. 12.

For the maximum power tracking (MPPT) curve of variable-speed wind turbine [12], tests for a complete generation system are carried out. The DFIG is set in power control. Given a rotor-speed measurement using an encoder, active power references are calculated from the MPPT curve and imposed on the DFIG after compensating for the power losses. Fig. 13 shows the experimental result when the rotor speed changes from 1480 to 1550rpm. In Fig. 13, the generation system operated well and achieved the MPPT curve during rotor speed variation.

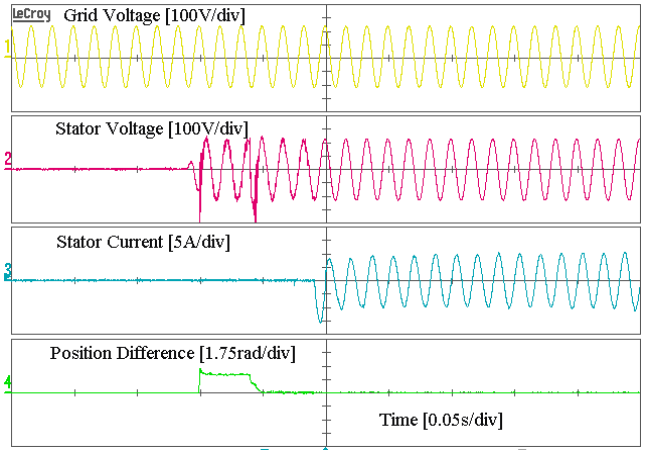

Fig. 11. Experimental results of the connection to the grid.

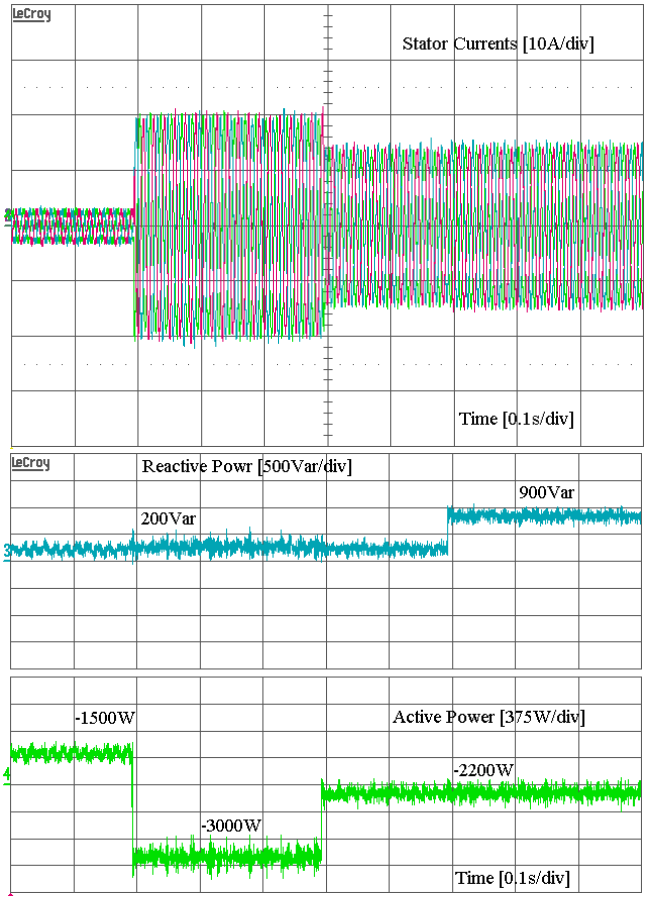

Fig. 12. Experimental results of the proposed DPC step responses.

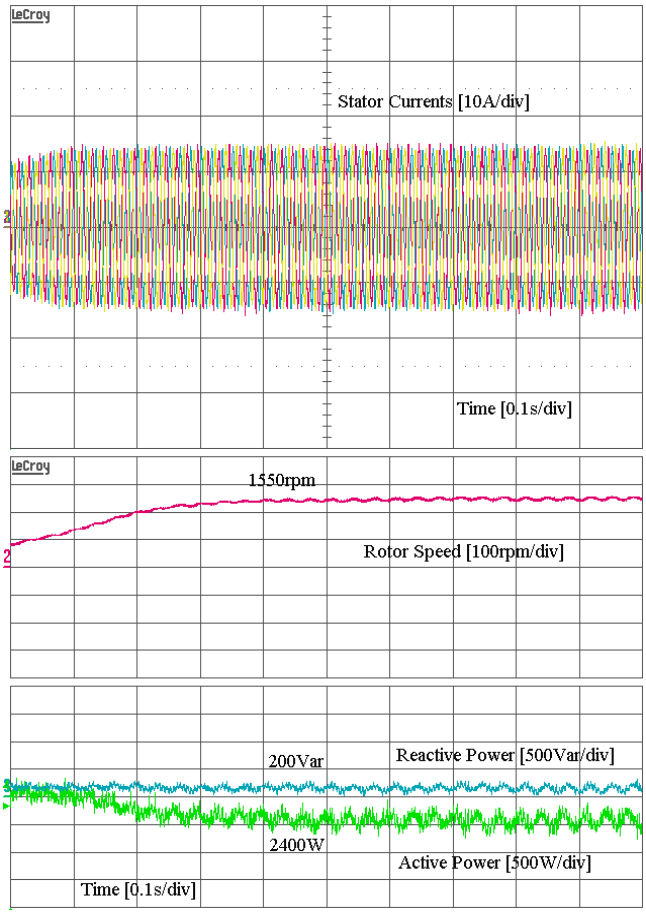

Fig. 13. Experimental results of a complete generation system.

VI. Conclusion

A direct power control method for DFIG drives was proposed to control the active and reactive powers directly without frame transformation and current controller used in the FOC drive, and achieve robustness. Simulated results and experimental results show the validity of the DPC algorithm with a fixed switching frequency. Comparing the FOC drive, the proposed control strategy can provide fasts dynamic response under transient conditions and robust characteristic against parameter variation.

References

[1] T. Ackermann, *Wind Power in Power Systems*. John Wiley and Sons, 2005.

[2] I. Boldea, *Electric Drives*. Taylor & Francis, 2006.

[3] S. Arnalte, J. C. Burgos and J. L. R. Amenedo, "Direct Torque Control of a Doubly-Fed Induction Generator for Variable Speed Wind Turbines," *Electric Power Components and Systems*, vol. 30, pp. 199-216, 2002.

[4] K. P. Gokhale, D. W. Karraker, and S. J. Heikkila, "Controller for a Wound Rotor Slip Ring Induction Machine," *U. S. Patent*, no. US2003/0071596, Apr. 2003.

[5] K. -B. Lee, C. -H. Bae, and F. Blaabjerg, "An improved DTC-SVM method for matrix converter drives using a deadbeat scheme," *International Journal of Electronics*, vol. 93, no. 11, pp. 737-753, Nov. 2006.

[6] K, -B. Lee and F. Blaabjerg, "Improved Direct Torque Control for Sensorless Matrix Converter Drives with Constant Switching Frequency and Torque Ripple Reduction," *International Journal of Control, Automation, and Systems*, vol. 4, no. 1, pp. 113-123, Feb. 2006.

[7] R. Datta and V. T. Ranganathan, "Direct Power Control of Grid-Connected Wound Rotor Induction Machine without Rotor Position Sensors," *IEEE Transactions on Power Electronics*, Vol. 16, No. 3, May 2001.

[8] M. Malinowski, M. P. Kazmierkowski, S. Hansen, F. Blaabjerg, and G. D. Marques, "Virtual-flux-based direct power control of three-phase PWM rectifiers," *IEEE Transactions on Industry Applications*, vol. 37, no. 4 pp. 1019-1027, Jul./Aug. 2001.

[9] A. Tapia, G. Tapia, J. X. Ostolaza, and Jose Ramon Saenz, "Modeling and Control of a Wind Turbine Driven Doubly Fed Induction Generator," *IEEE Transactions on Energy Conversion*, vol. 18, no. 2, pp. 194-204, June 2003.

[10] Y. Lei, A. Mullane, G. Lightbody, and R. Yacamini, "Modeling of the Wind Turbine With a Doubly Fed Induction Generator for Grid Integration Studies," *IEEE Transactions on Energy Conversion*, vol. 21, no. 1, Mar. 2006.

[11] G. Tapia, A. Tapia, J. X. Ostolaza, "Two Alternative Modeling Approach for the Evaluation of Wind Farm Active and Reactive Power Performances,," *IEEE Transactions on Energy Conversion*, vol. 21, no. 4, pp. 909-920, Dec. 2006.

[12] L. Mihet-Popa, F. Blaabjerg and I. Boldea, "Wind Turbine Generator Modeling and Simulation Where Rotational Speed is the Controlled Variable" *IEEE Transactions on Industry Applications*, vol. 40, no. 1, pp. 3-10, Jan/Feb. 2004.